nature chemistry

SUPPLEMENTARY INFORMATION

https://doi.org/10.1038/s41557-020-0511-7

In the format provided by the authors and unedited.

De novo engineering of intracellular condensates using artificial disordered proteins

Michael Dzuricky[1], Bradley A. Rogers[2], Abdulla Shahid[3,4], Paul S. Cremer[2] and Ashutosh Chilkoti[1]✉

[1]Department of Biomedical Engineering, Duke University, Durham, NC, USA. [2]Department of Biochemistry and Molecular Biology, Pennsylvania State University, University Park, PA, USA. [3]Department of Computer Science, Duke University, Durham, NC, USA. [4]Department of Biology, Duke University, Durham, NC, USA. ✉e-mail: chilkoti@duke.edu

Supplementary Information File

De Novo Engineering of Intracellular Condensates using Artificial Disordered Proteins

Authors: Michael Dzuricky[1] , Bradley A. Rogers[2], Abdulla Shahid[3,4], Paul S. Cremer[2], Ashutosh Chilkoti[1*]

Table of Contents:

Extended Materials and Methods:

Materials: pET24+ vectors were purchased from Novagen (Madison, WI). gBlock fragments encoding repetitive IDP (A-IDP) sequences of interest, superfolder GFP (sfGFP), mRuby3 and primers for pcDNA5 vector were purchased from Integrated DNA Technologies (Coralville, IA). Ligation enzymes, restriction enzymes, DNA ladders were purchased from New England Biolabs (Ipswich, MA). BL21 (DE3) chemically competent Escherichia coli (E. coli) cells were purchased from Bioline (Taunton, MA). All E. coli cultures were grown in Terrific Broth media purchased from VWR International (Radnor, PA). Kanamycin sulfate was purchased from EMD Millipore (Billerica, MA). Protein expression was induced with isopropyl β-D-1-thiogalactopyranoside (IPTG) from Gold Biotechnology (St. Louis, MO). All salts, 10/40kDa fluoresceine labeled dextran molecules, L-(+)-Arabinose, L-Rhamnose and Fluorescein di(β-D-galactopyranoside) were purchased from Sigma-Aldrich (St. Louis, MO). 1X phosphate buffered saline (PBS) tablets (10 mM phosphate buffer, 140 mM NaCl, 3 mM KCl, pH 7.4 at 25 °C) were purchased from EMD Millipore (Billerica, MA). KRX E. coli cell line that endogenously expresses mutated LacZ were purchased from Promega (Madison, WI). NHS Ester reactive fluorophores (NHS-Alexa Fluor® 350 & NHS-Alexa Fluor® 647) were purchased from Life Technologies (Grand Island, NY). DNA extraction kits, DNA gel purification kits were purchased from Qiagen Inc. (Germantown, MD). Expi293 Eurkaryotic Expression System for HEK293 expression was purchased from Thermo Fischer Scientific (Waltham, MA). Whatman Anotop sterile syringe filters (0.02 μm) were purchased from GE Healthcare Life Sciences (Pittsburgh, PA). ABIL® EM 90 and TEGOSOFT® DEC surfactants were purchased from Evonik Industries (Essen, Germany). A single emulsion droplet-generating chip was purchased from Dolomite Microfluidics (Royston, United Kingdom). Syringe pumps were acquired from Chemyx Inc. (Stafford, TX).Image Quantification and Statistical Analysis: For experiments performed with regard to determining the intracellular fluorescent intensity of A-IDP-sfGFP at various points post-IPTG induction the following statistical analysis was performed. For determining the saturation concentration intracellular, whole cell fluorescence normalized to cellular density (OD_{600}) on three independent samples was calculated alongside of imaging of their intracellular architecture. Upon first observation of phase separation in *E. coli* in more than

50% of cells within a microscopic field of view, this normalized cell density was recorded as the saturation concentration. Data is normalized to data collected for [WT]-40 as a reference point. Error bars represent propagated standard error of the mean of three separate samples from the same original cell suspension.

With the microscope images collected with confocal microscopy at various time points, we isolated the soluble and puncta fractions within the cells at various points in time via analysis in ImageJ. Puncta consistently create pixels dense enough to saturate the detector while simultaneously observing the rest of the cell. Thus, by thresholding around the upper 2% of total pixel intensities, one can easily partition this section from the remaining cell cytoplasm. Using this constant thresholding between timepoints in each experimental group, we were able to track the total size of these puncta over time with regard to the total size of the cell (puncta + soluble fraction). Error bars of these data are standard errors of the mean of normalized puncta (two-phase) area of three images of different fields of view of the sample overall cell samples. These two channels are combined and split differently in supplementary figure 15 but have the same thresholding process applied to each image.

Given the lack of automated tools for the detection of intracellular phase separation between two images, we calculated the intracellular transition temperatures manually. Similar to the detection of phase separation with UV-Vis spectrophotometry, the intracellular transition temperature was determined as the midpoint between a frame that was certainly homogenous and a second frame that was certainly two phases. All transition temperatures were determined in this way, going from a point of solubility to insolubility whether the solution was being heated or cooled. Due to the level of subjectivity of this assessment, sample identifiers were blinded to the analyst and a high number of cells were analyzed in each experiment (n = 30). Data was normalized to the initial mean fluorescence of the homogeneous cells at a consistent temperature (often 60^0C unless otherwise noted). Error bars indicate standard error of the mean.

The error bars of dextran fluorescence indicate the standard error of the mean fluorescence inside and outside of the phase separated space from three separate fields of view.

For quantification of Fluorescein Di-β-D-Galactopyranoside (FDG) relative to the different expression levels of alpha peptide, channels were split between fluorescence from FDG and mRuby3 respectively. Using

the particle analysis tool from ImageJ, areas of green fluorescence were isolated from the background. If the mean fluorescence of this area was 5% greater than the background fluorescence (mean fluorescent of the area excluded by the previous particle mask), then this particular particle's background subtracted green fluorescence was included in the analysis. Particles were excluded if their area was below 0.1 um^2. Using the same particle mask, the background subtracted mean fluorescence of mRuby3 was calculated on the other fluorescent channel. We report the ratio of these two channels as a surrogate for enzymatic efficiency. Error bars are standard errors of the mean at each timepoint.

For quantification of Fluorescein Di-β-D-Galactopyranoside (FDG) inside the cellular space versus outside the cellular space, channels were first split between fluorescence from FDG and mRuby3 respectively. Using the same particle analysis tool from ImageJ, areas of green fluorescence were isolated from the background. If the mean fluorescence of this area was 5% greater than the background fluorescence (mean fluorescent of the area excluded by the previous particle mask), then this particular particle's background subtracted green fluorescence was included in the analysis. Particles were excluded if their area was below 0.1 um^2. Ratio of fluorescent intensity inside of cells versus the extracellular space is the background corrected mean fluorescence of FDG divided by the background fluorescence. Error bars are standard errors of the mean at each timepoint.

To quantify the amount of colocalization we used the Coloc2 plug-in available through ImageJ software. Using automated thresholding, we report the Mander's colocalization coefficient which accounts for the intensity to the two channels of interest.

Supplementary Figures:

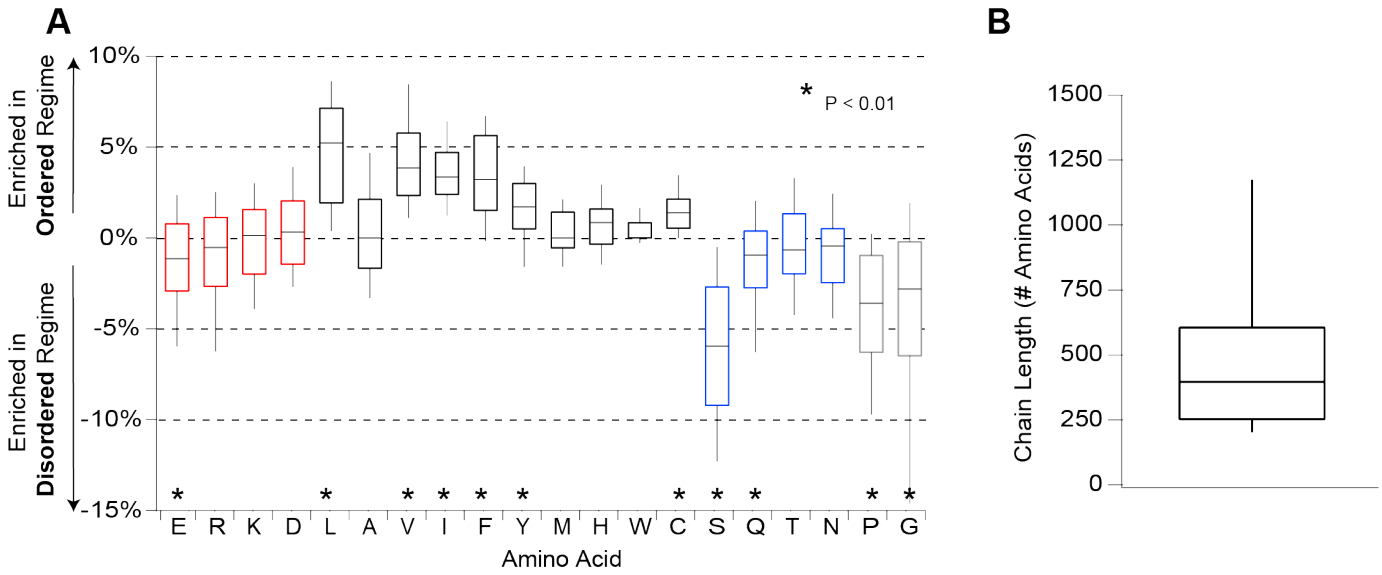

Supplementary Fig. 1. Additional Proteomic Analysis Related to Fig. 1. a. Graph of the difference in amino acid composition between ordered and disordered regions within the same protein. A disordered region was defined as being scored with a >0.5 value using PONDR VSL2, ordered regions with a score of <0.5. Values were calculated by subtracting the percentage of chain composition in disordered regime from ordered regime. Bars indicate 25th-75th percentiles and whiskers indicate 10th-90th percentiles. Middle line indicates the median of the data set. N = 63, * $P < 0.01$ in students t-test between ordered and disordered regions of all proteins sampled. **b.** Histogram plotting the length of the disordered regions analyzed in this study. Bars indicate 25th-75th percentiles and whiskers indicate 10th-90th percentiles.

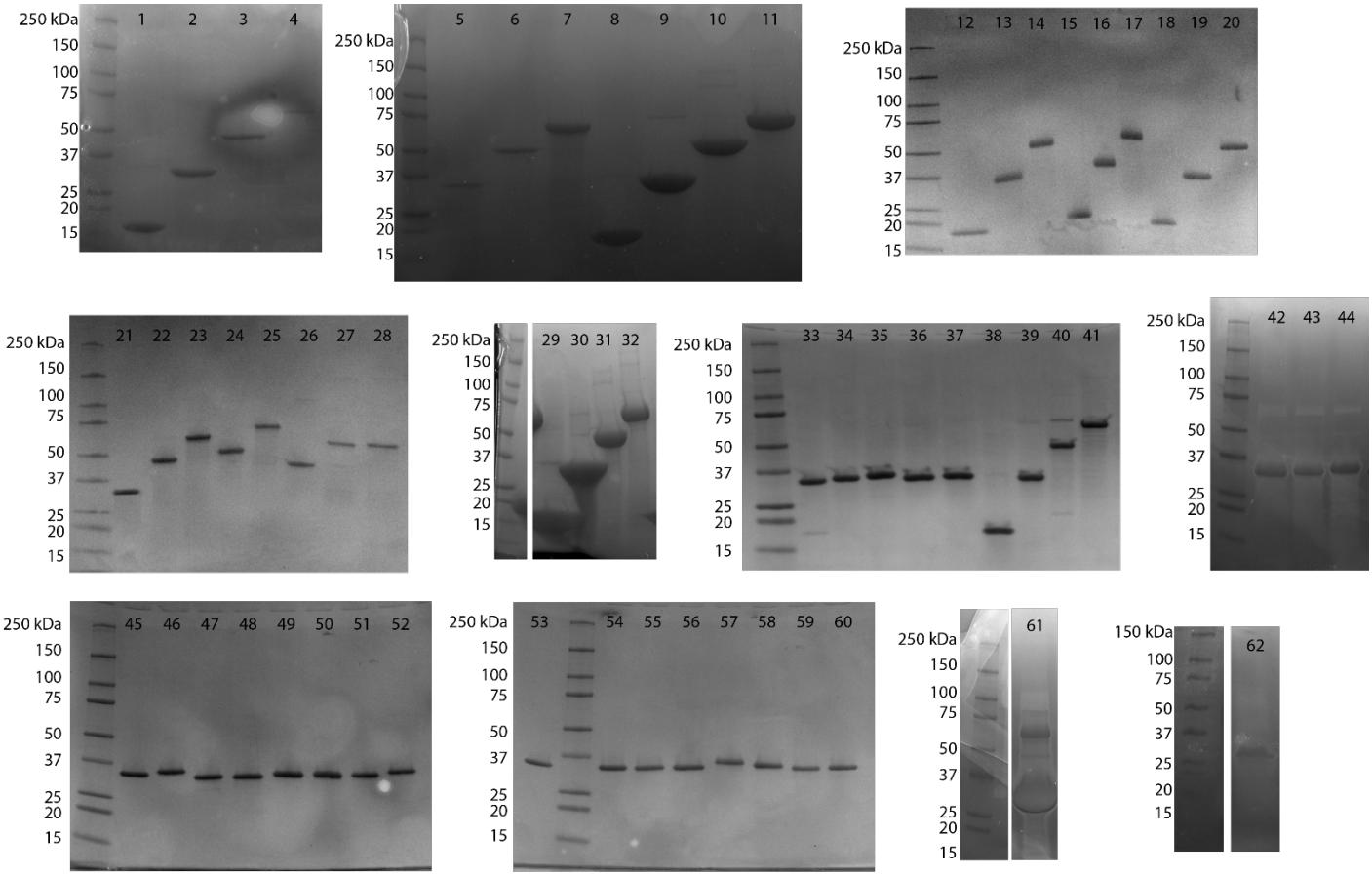

Supplementary Fig. 2. SDS-PAGE Gels of Purified Proteins Used in this Study Relevant to Fig. 1-5. Lane labels for each protein purified in this study are listed in Supplementary Table 1 and Supplementary Table 2.

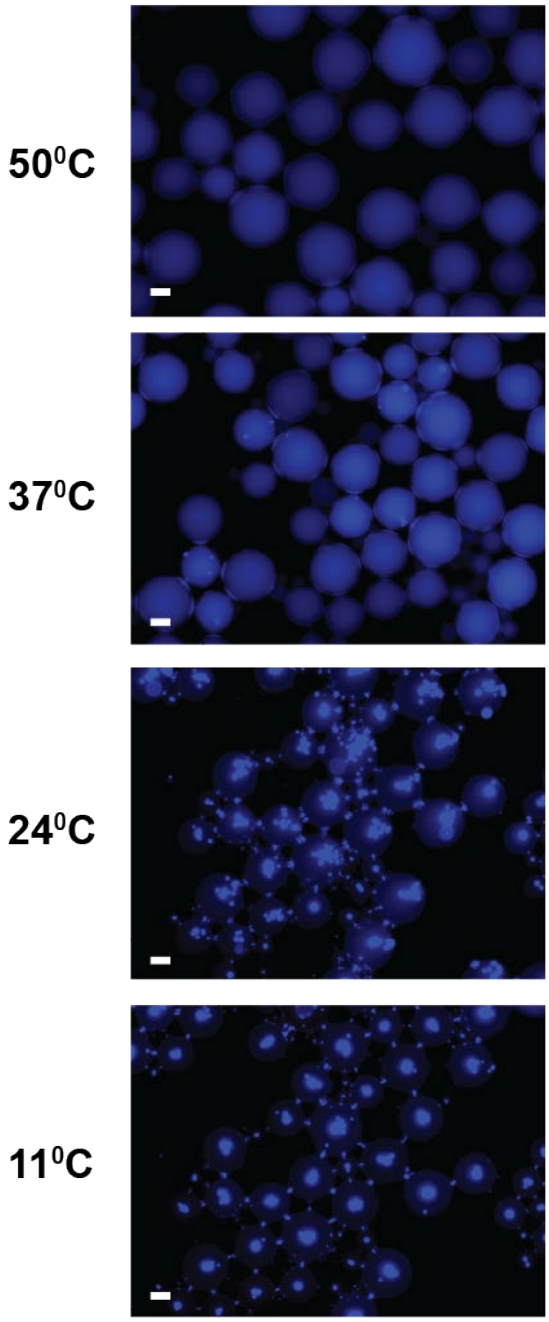

Supplementary Fig. 3. Wide-field Fluorescent Microscope Images of Fluorescently Labeled [$Q_{5,8}$]-20 Inside Water-in-Oil Compartments Related to Fig. 1. [$Q_{5,8}$]-20 was labeled with AlexaFluor 350 via NHS chemistry and resuspended in 140 mM PBS at pH 7.4 to a final ϕ = 0.0018 (100 μM). Water-in-oil mixture was transferred to glass slide and cooled from 50°C to 10°C. Scale bar = 20 μm.

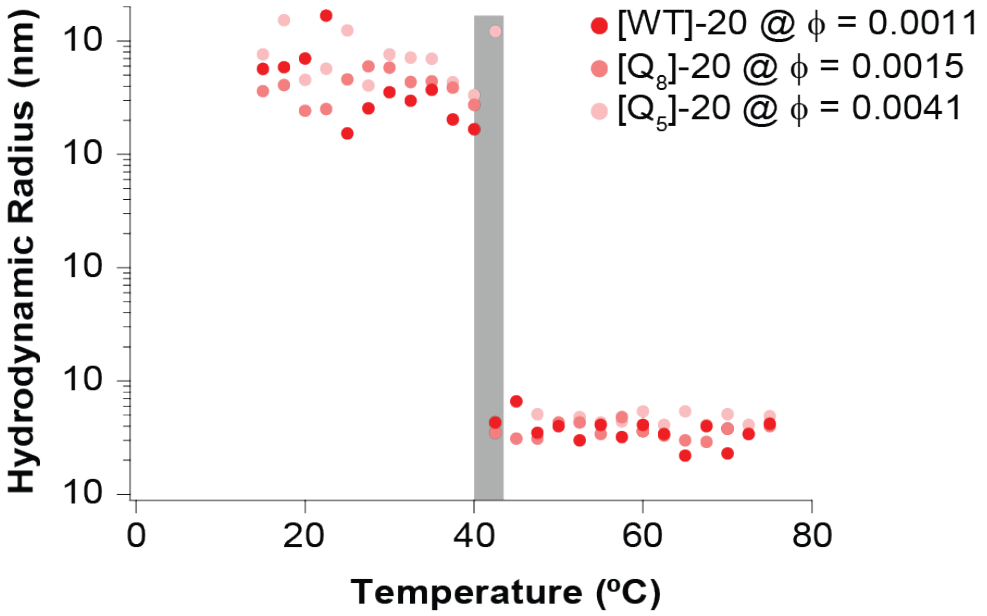

Supplementary Fig. 4. Additional Dynamic Light Scattering Data Related to Fig. 1. Data collected on 20 nm filtered samples at volume fractions that were predicted to exhibit liquid-liquid phase separation at 40˚C. Data collected in 140 mM PBS, pH 7.4. ϕ = 0.0011 (65 μM), ϕ = 0.0015 (84 μM), ϕ = 0.0041 (230 μM).

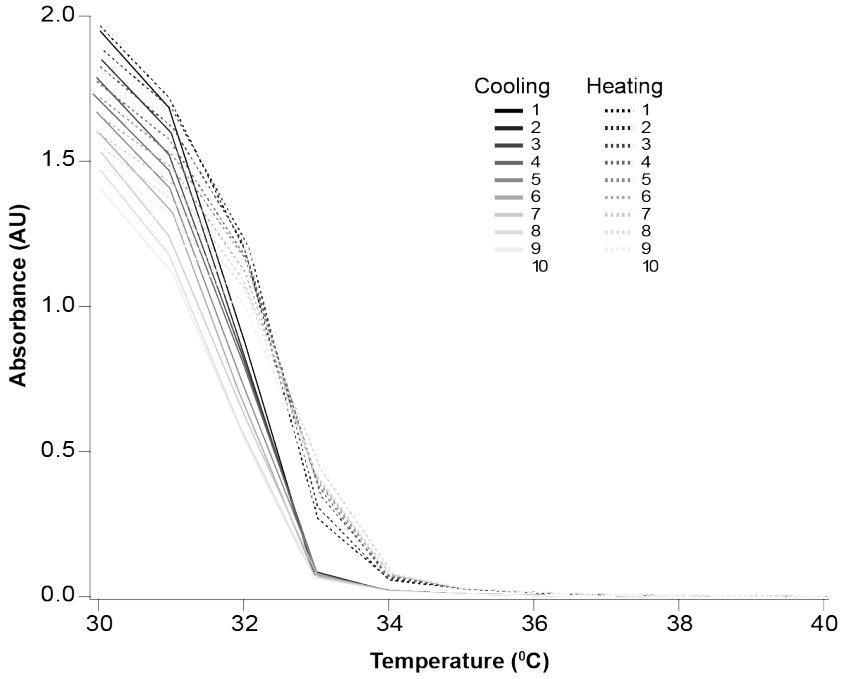

Supplementary Fig. 5. Cyclic Cooling and Heating Cycles Exhibit Minimal Hysteric Behavior Related to Fig. 1. Optical turbidity measured at 350 nm of repeated cooling and heating curves of [$Q_{5,8}$]-20 @ ϕ = 0.0025 between 40˚C and 30˚C.

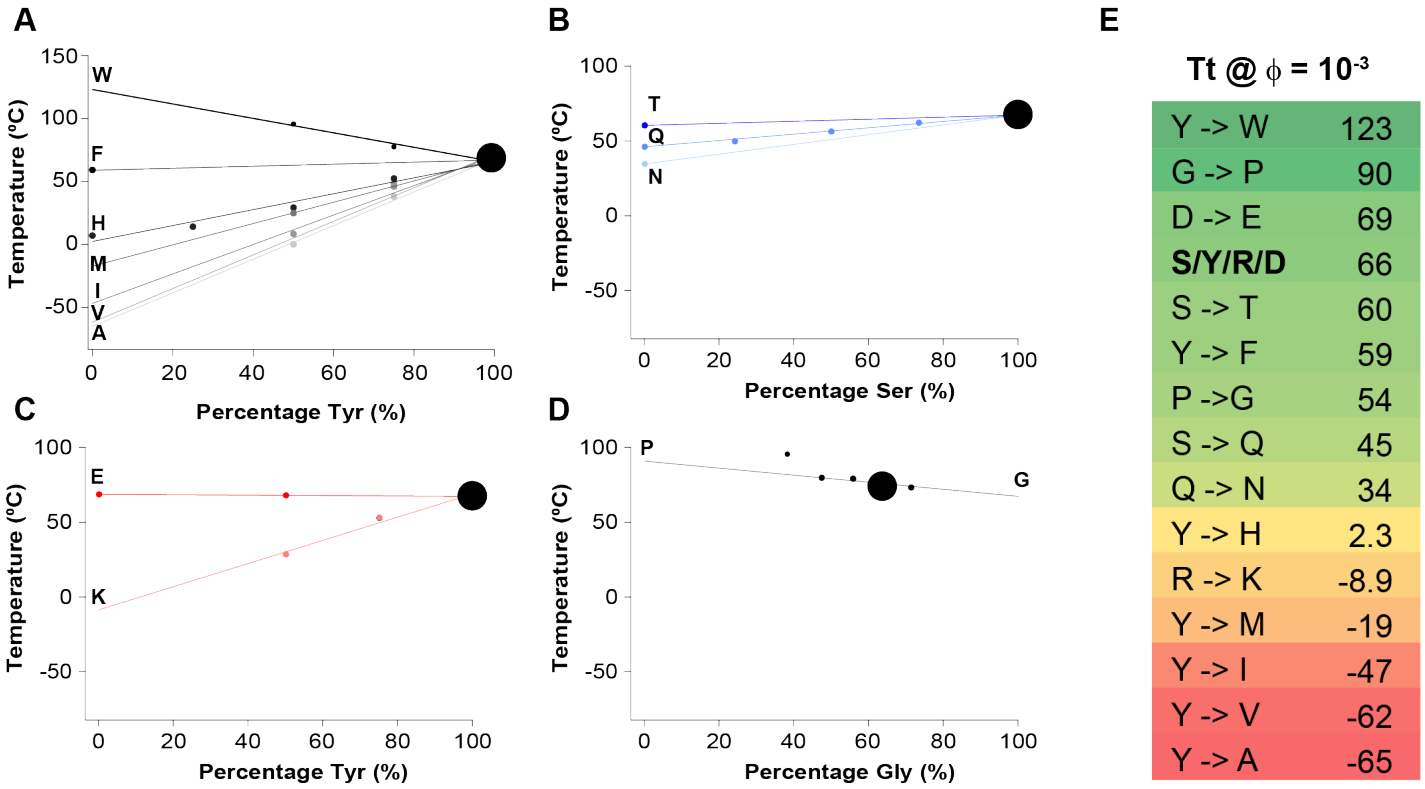

Supplementary Fig. 6. Effect of Single Amino Acid Substitutions on UCST Cloud Point and New Relative UCST Propensity Scale Related to Fig. 2. **a.** Partial binodal phase boundary of well-mixed, di-block polypeptides with varied ratio of aromatic:aliphatic residues. **b.** Partial binodal phase boundary of well-mixed, di-block polypeptides with varied ratio of polar non-charged residues. **c.** Partial binodal phase boundary of well-mixed, di-block polypeptides with varied identity of positively charged and negatively residues. **d.** Partial binodal phase boundary of well-mixed, di-block polypeptides with varied amount of. Data collected under physiologic solution conditions (140 mM PBS, pH 7.4) at $\phi = 10^{-3}$ (25-30 μM). All polypeptides are 326 amino acids in length. **e.** A relatively scale for UCST propensity based on substitutions made to the [WT] repeating motif. The transition temperatures listed are the UCST cloud point at $\phi = 10^{-3}$ (25-30 μM) if the left amino acid was replaced with the amino acid to the right of the arrow and the total number of amino acids was 326.

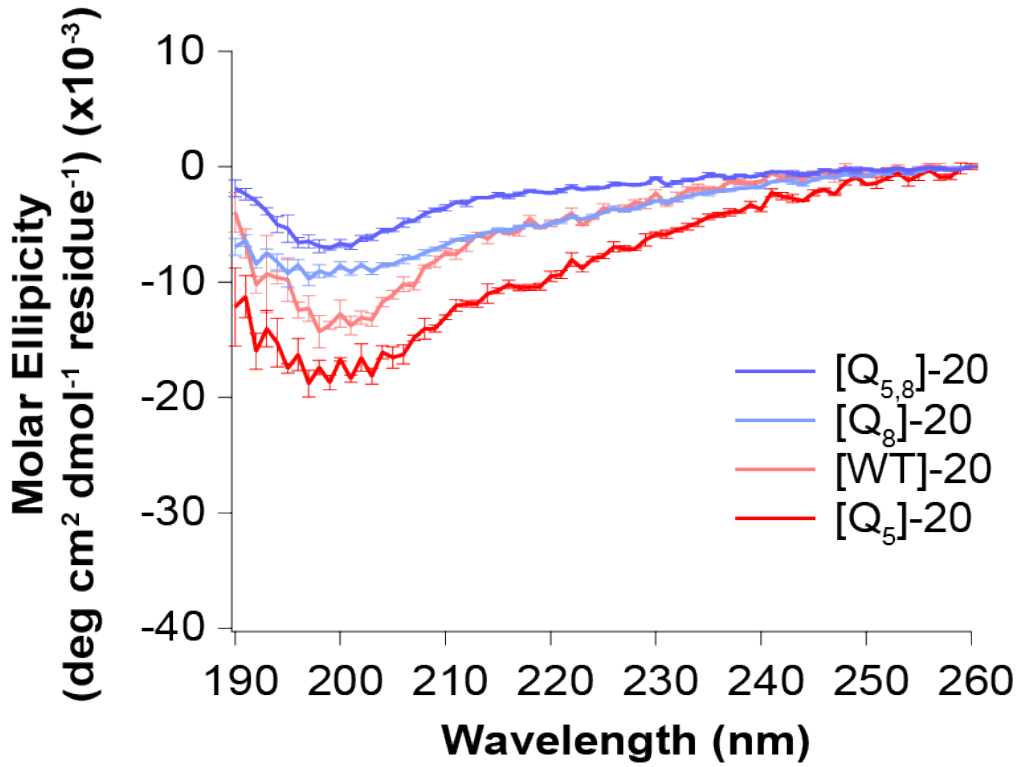

Supplementary Fig. 7. Analysis of Secondary Structure with Circular Dichroism (CD) Spectroscopy

Related to Fig. 2. CD spectra of various A-IDPs lack a defined secondary structure curve shape, characteristic of other IDP and other repetitive protein polymers. Data collected at 50°C (soluble chains) at 5 μM in 5 mM PBS, pH 7.4. Error bars indicate standard deviation of three sequential runs.

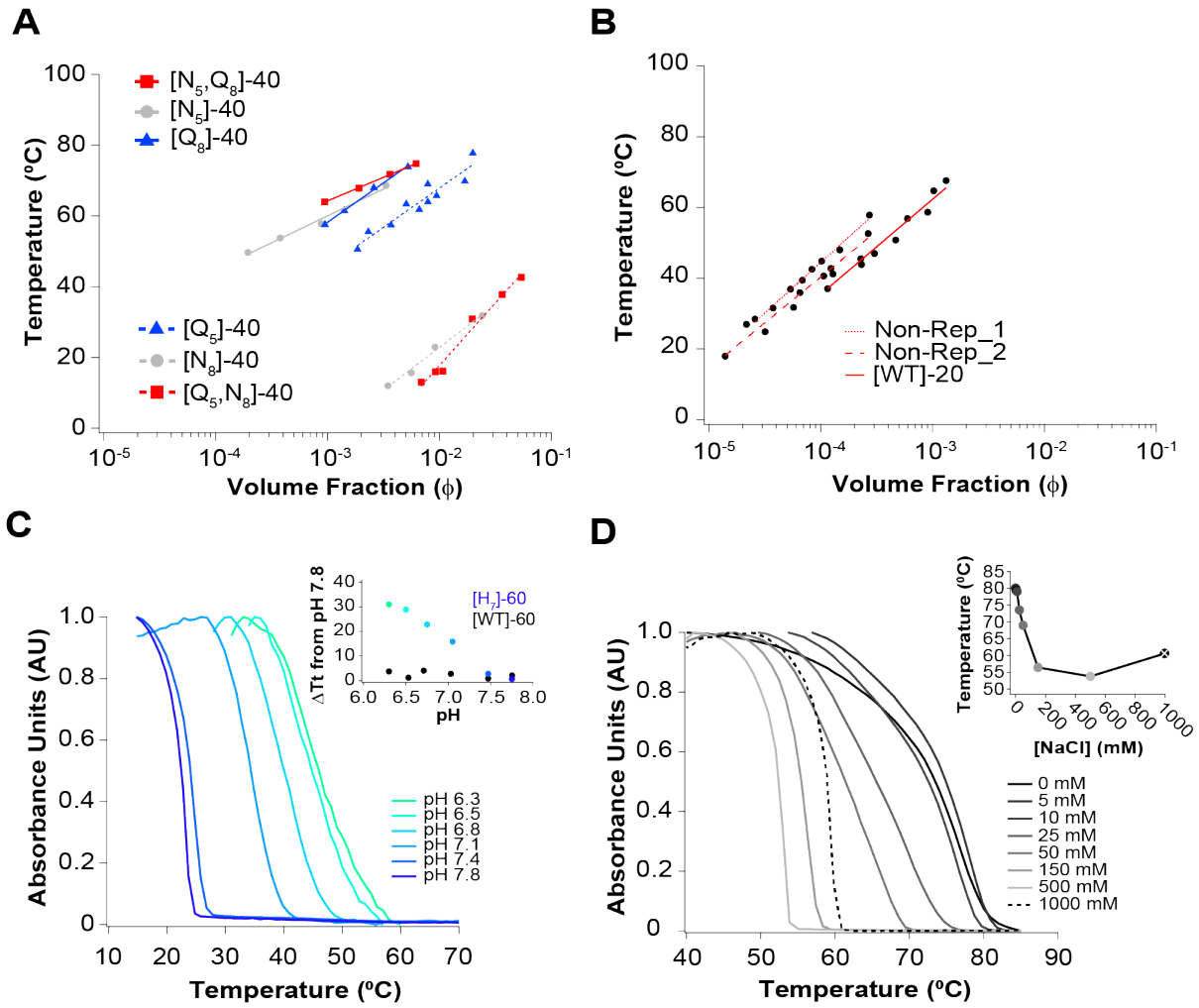

Supplementary Fig. 8. Minor Effects on UCST Cloud Point in Protein Polypeptides Related to Fig. 2. a. Partial binodal phase diagram of sequence syntax permutations focused around the Pro residue. Mutations reveal that amino acid mutation site affects the UCST binodal, particularly at the fifth position, but do not eliminate phase behavior. Data collected under physiologic conditions (140 mM PBS, pH 7.4). **b.** Partial binodal phase boundaries of agnostically non-repetitive but compositionally identical versions of [WT]-20. **c.** Turbidity curves of [H_7]-60 in different pH solutions. Decreasing the pH and protonation of the His residues increases and broadens observed UCST phase behavior. This effect centers at ~ pH 7, very close to the predicted pKa of the imidazole group in H. In contrast to, [WT]-60's UCST cloud point does not change as a function of pH (black dots, graph insert). **d.** Turbidity curves of [$Q_{5,8}$]-40 in solutions with different concentrations of NaCl. In pure water, [$Q_{5,8}$]-40 exhibits a broad transition at higher temperatures. Increasing the concentration of NaCl

between 0-140 mM reduces and sharpens the UCST cloud point, finally reaching a minimum at ~500 mM. From this point, the protein exhibits a salting-out effect and the transition temperature begins to rise again.

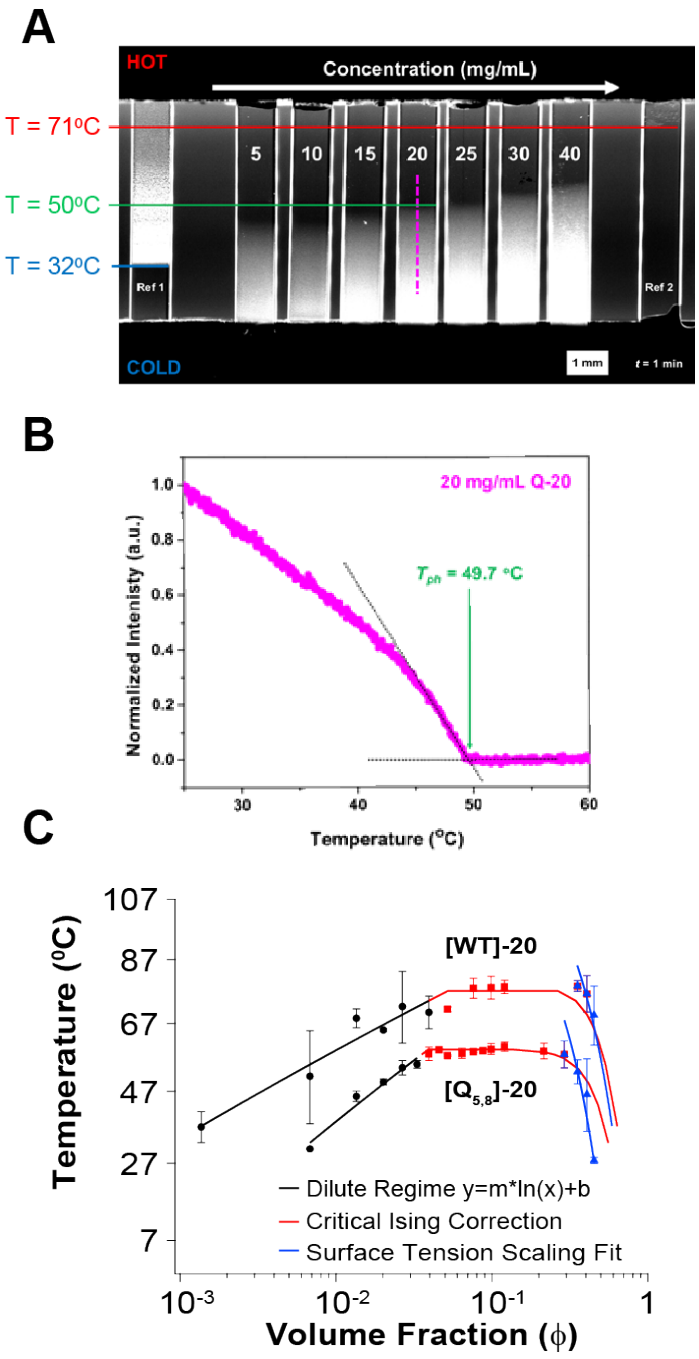

Supplementary Fig. 9. Mapping Phase Diagrams Using A Temperature Gradient Device Related to Fig. 2. a. Representative dark-field image of [$Q_{5,8}$]-20 solutions on a temperature gradient device. The transition temperatures of the reference solutions (red and blue lines) and the 20 mg ml^{-1} [$Q_{5,8}$]-20 solution (green line)

are indicated by the horizontal colored lines. The dashed vertical magenta line along the 20 mg ml^{-1} capillary tube illustrated the region of the image used to measure the line scan. **b.** Line scan of normalized light scattering intensity versus temperature for the 20 mg ml^{-1} [$Q_{5,8}$]-20 capillary shown in a. The dashed black lines represent tangent lines for the high temperature baseline and increase in light scattering at lower temperatures. These two lines intersect at T_{ph}, as indicated by the vertical green line. **c.** Final binodal phase lines of [WT]-20 and [$Q_{5,8}$]-20 using multiple data points from temperature gradient device. A three-piece fit was utilized to fit three regimes that roughly correspond to the dilute, overlap, and semi-dilute regimes of the polypeptide phase diagram. The observed data and subsequent fits demonstrate that polypeptide sequence not only affects UCST cloud point in the dilute regime but over the entire concentration range measured ($\phi \leq 0.5$)

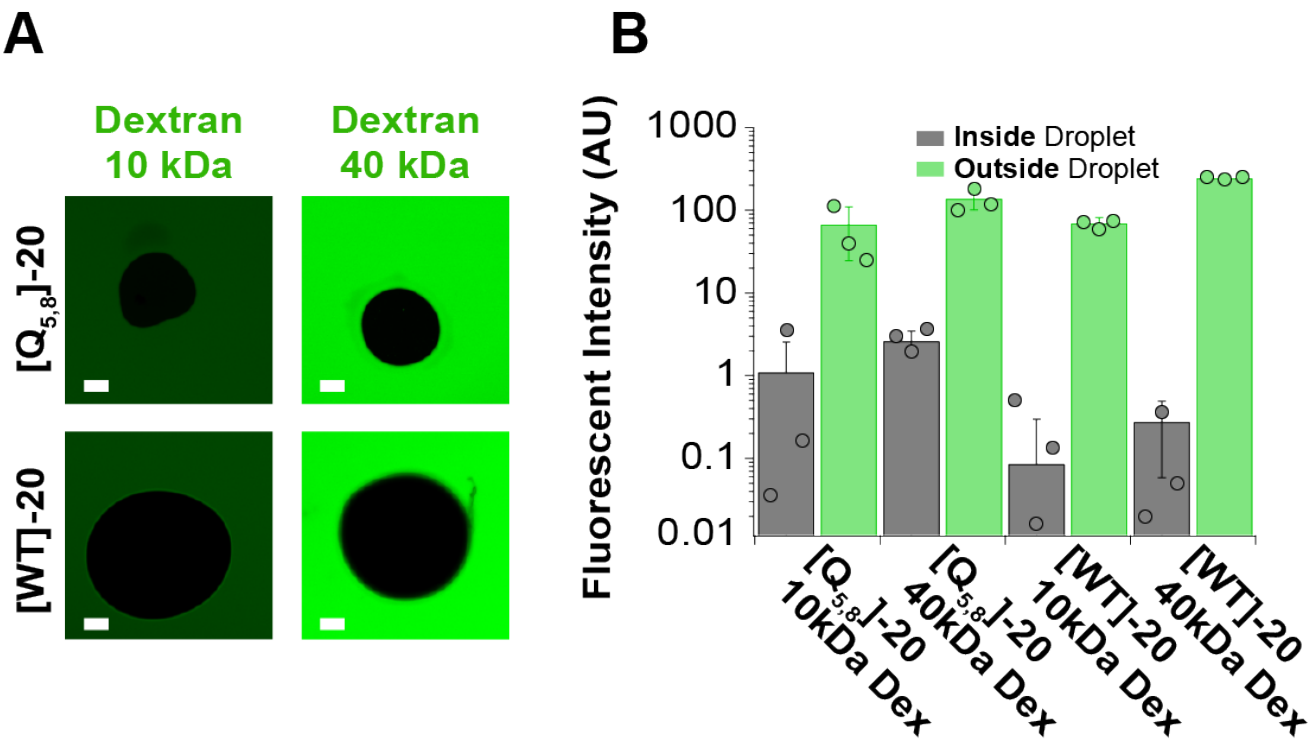

Supplementary Fig. 10. Quantification of Dextran Uptake During Phase Separation of A-IDPs Related to Fig. 1. a. Fluorescent microscopy images of phase separated droplets in the presence of dextran molecules of different molecular weight (10/40kDa) labeled with Alexa488 (green) fluorophore. Inside the phase separated space (dark circles), there is very little sequestration of the dextran molecules as a function of dextran molecular weight or A-IDP sequence. Scale bar is 20 μm. **b.** Quantification of fluorescent signal between the area inside of phase separated droplets and outside. n = 3, error bars represent standard deviation of the mean.

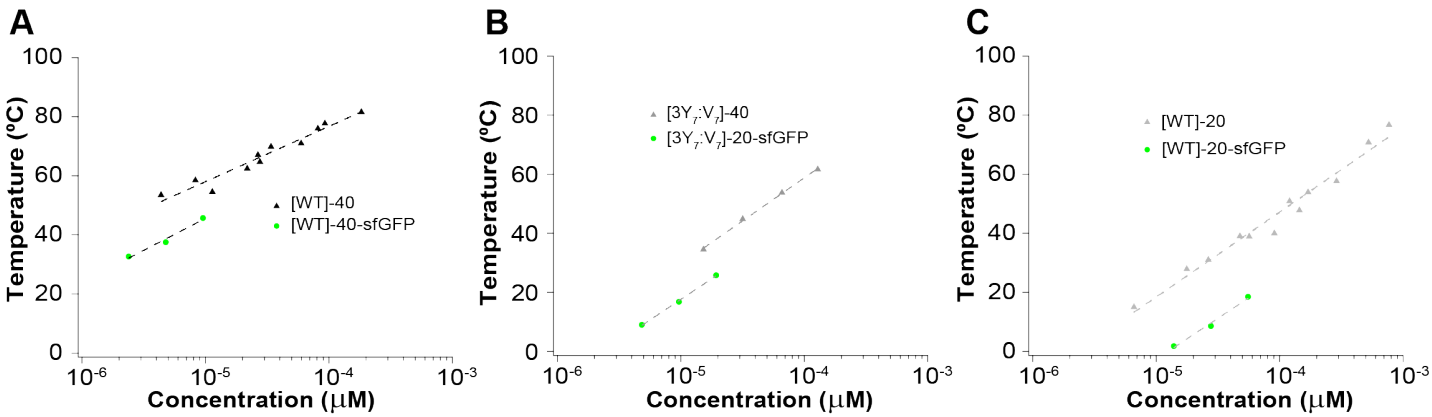

Supplementary Fig. 11. Comparison of Partial Binodal Phase Diagrams of A-IDP and A-IDP–sfGFP Fusions Related to Fig. 4. **a.** Partial binodal phase boundaries of [WT]-40 and [WT]-40-sfGFP. **b.** Partial binodal phase boundaries of [$3Y_7$:V_7]-40 and [$3Y_7$:V_7]-40–sfGFP. **c.** Partial binodal phase boundaries of [WT]-20 and [WT]-20-sfGFP. The sfGFP fusion lowers the UCST binodal line for all A-IDPs. These data suggest that the larger molecular weight polypeptides are less affected by sfGFP fusion as the observed difference in [WT]-40 and [$3Y_7$:V_7]-40 is a only ~10°C instead of ~20°C for [WT]-20.

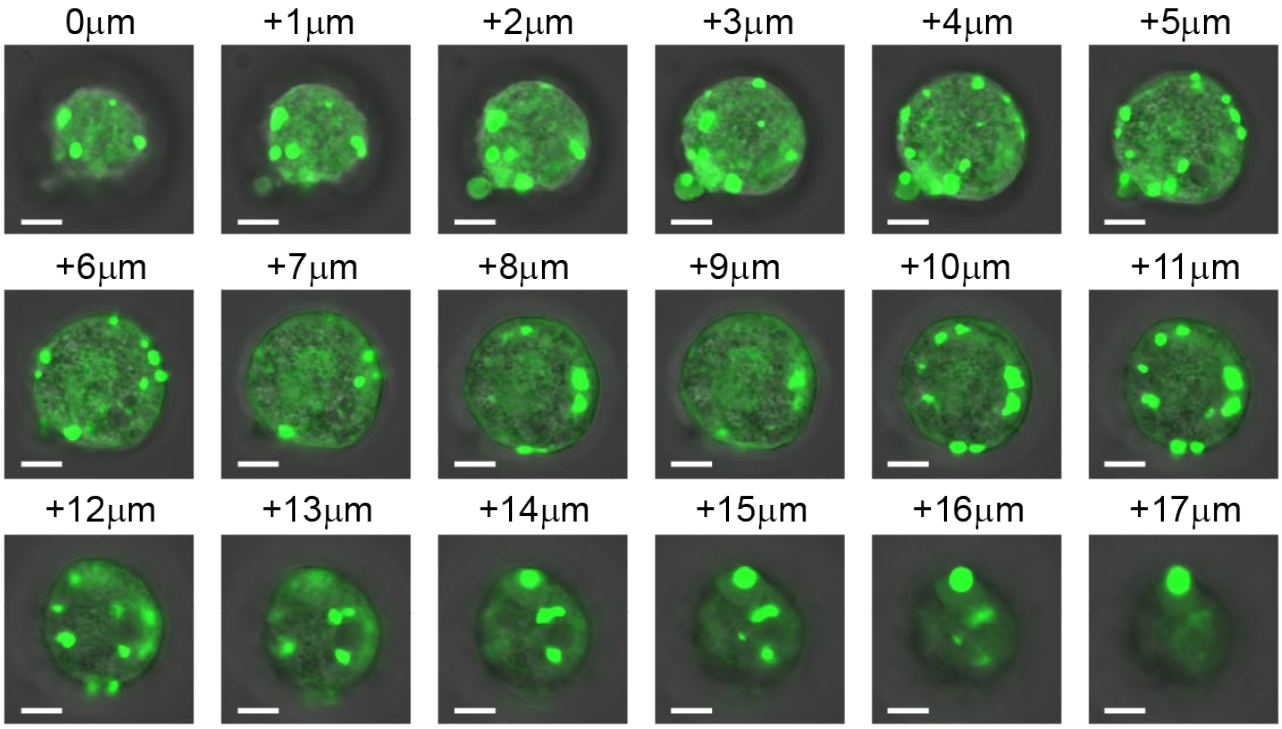

Supplementary Fig. 12. Additional Confocal Microscopy Images of HEK293 Cells with Transiently Transfected [WT]-20-sfGFP Related to Fig. 4. Confocal fluorescence image slices throughout the cell demonstrate that phase separated droplets are formed throughout the cytoplasm without obvious colocalization with other cellular structures. Images taken 24 hrs after transfection with 3 μg of pCDNA plasmid that encode [WT]-20–sfGFP. Scale bar = 5 μm. Data collected from a single transfection population.

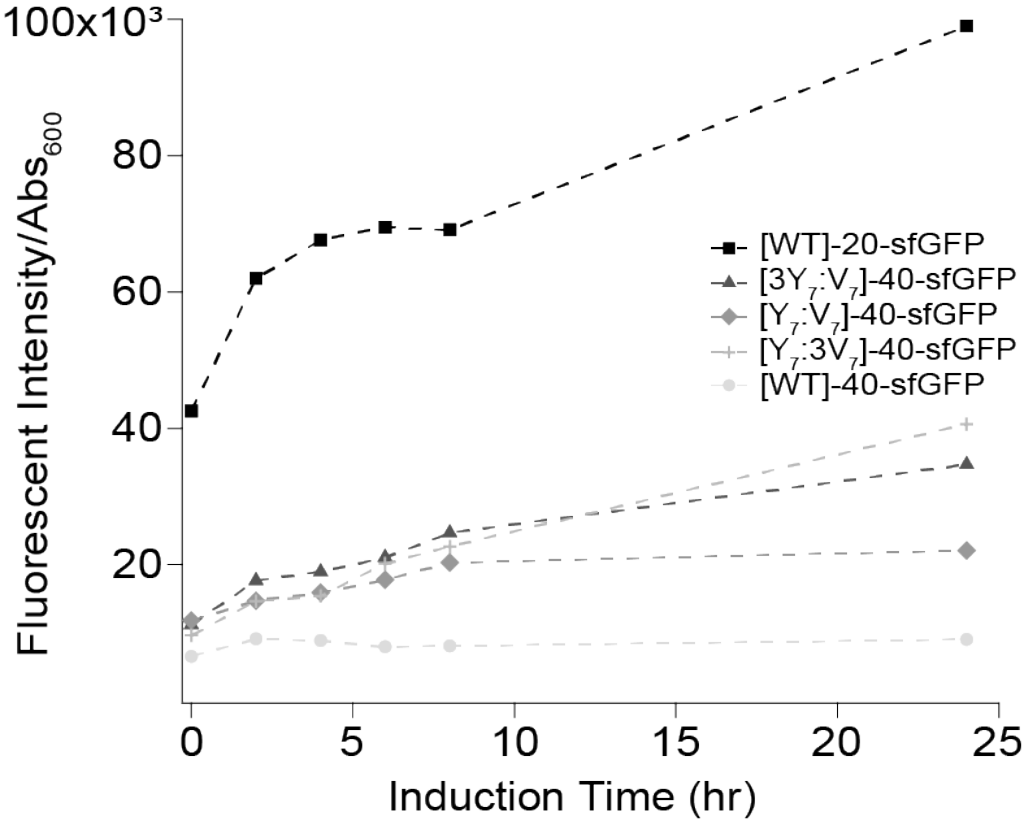

Supplementary Fig. 13. Measurement of Total Cellular Fluorescence as a Function of Time Post Induction Related to Fig. 4. *E. coli* cultures were spun down and resuspended in 140 mM PBS, pH 7.4. The optical turbidity and fluorescence intensity of sfGFP were measured and plotted as a function of time. Data collected at 22 °C.

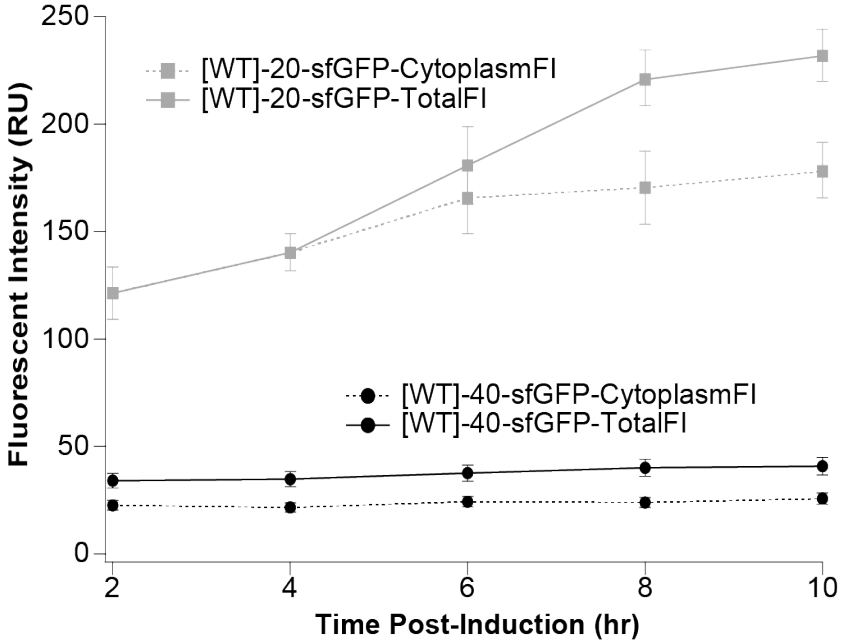

Supplementary Fig. 14. Measurement of the Cellular Fluorescence at Different Locations Within the Cell Related to Fig. 4. Digital partitions were made between the dense phase separated area of the cell and soluble cytoplasmic space using ImageJ. The mean of the total cell fluorescence intensity (solid line) and cytoplasmic fluorescence intensity (dotted line) are plotted as a function of time post-IPTG induction. [WT]-20–sfGFP does not exhibit intracellular droplets until the 6 hr mark. At this point the cytoplasmic fluorescence intensity remains constant but the total fluorescent increases from 6 hr onward. [WT]-40–sfGFP phase transitions prior to the 2-hr timepoint. Center points are the mean with standard error bars. n = 3.

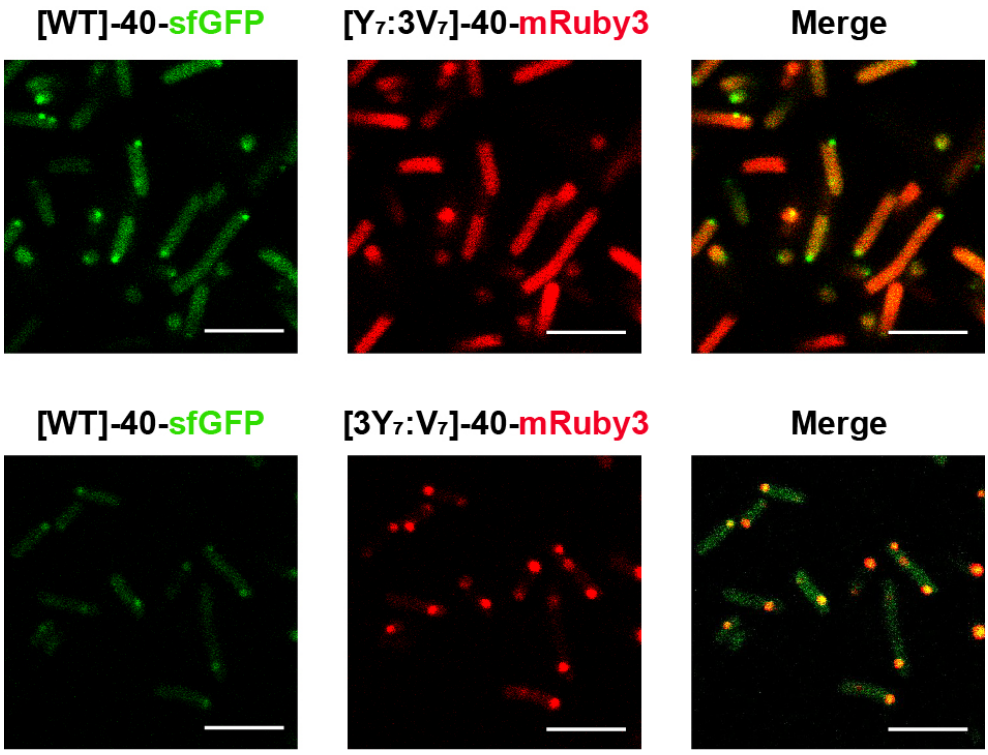

Supplementary Fig. 15. Confocal Fluorescence Microscope Images of *E. coli* Co-expressing Two A-IDP-Fluorescent Fusions Related to Fig. 4. Top: Co-expression of [WT]-40-sfGFP and [Y_7:3V_7]-40-mRuby3 results in the formation of isolated intracellular droplets of [WT]-40-sfGFP. Bottom: Conversely, co-expression of two proteins with relatively similar phase behavior, [WT]-40-sfGFP and [3Y_7:V_7]-40-mRuby3, results in colocalized droplets inside the bacterial cells. Data taken at 22°C. Scale bar = 5 μm.

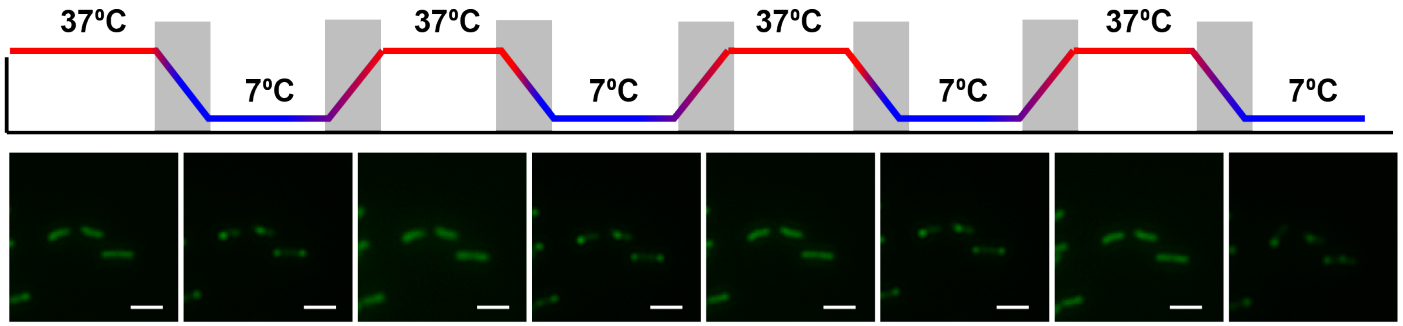

Supplementary Fig. 16. [WT]-20-sfGFP Exhibits Phase Separation Memory Upon Multiple Cycles of Heating and Cooling Related to Fig. 5. Upon multiple heating and cooling cycles, [WT]-20-sfGFP form puncta in the same location as the first cooling cycle. Given the importance of memory, it is critical to note that the observed transition temperature was below room temperature (~15˚C), suggesting that these cells are naïve to phase separation as they were incubated at 37˚C and processed at room temperature. Scale bar indicated 5 µm. Cooling and heating rate were set to a constant 5˚C min^{-1}.

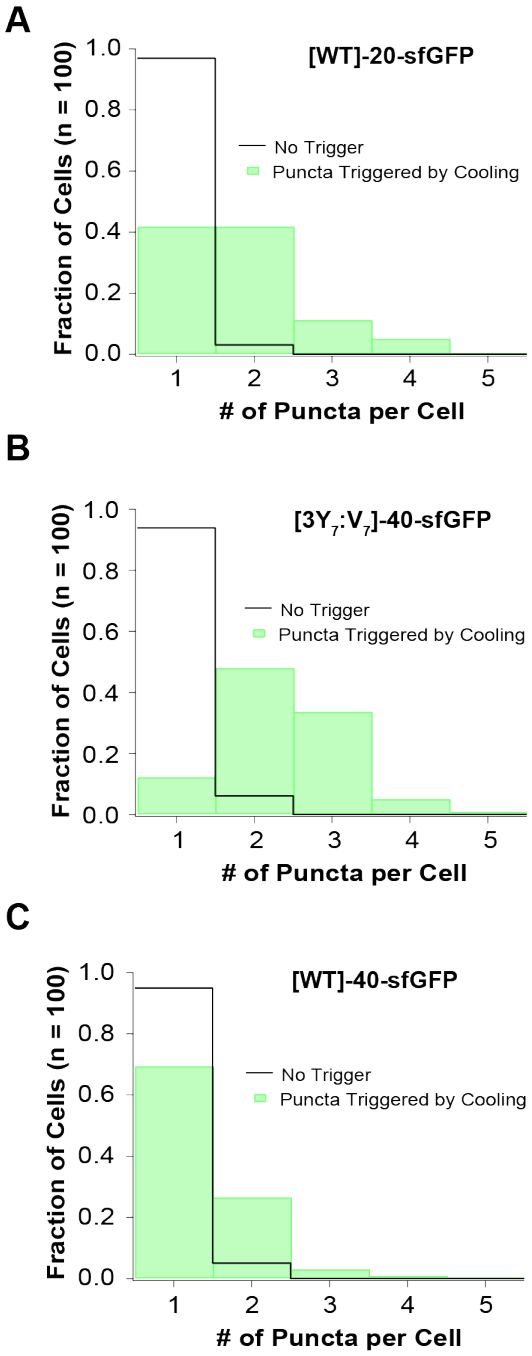

Supplementary Fig. 17. Image Analysis of the Number of Puncta Formed in Each Cell Related to Fig. 5. 100 cells at random were tabulated for each histogram. **a.** Number of intracellular puncta formed in each cell containing [WT]-20-sfGFP during a cooling ramp from 60˚C ➔10˚C (green) and imaged isothermally at 22˚C. Isothermal analysis performed at 6 hrs post induction, the first timepoint where intracellular puncta were observed. Cooling ramp performed at 4 hrs post induction, where transition temperature (T_t) was between 22˚C and 37˚C. **b.** Number of intracellular puncta formed in each cell containing [3Y:V]-40-sfGFP during a cooling

ramp from 60°C ➔10°C (green) and imaged isothermally at 22°C. Isothermal analysis performed at 4 hrs post induction, the first timepoint where intracellular puncta were observed. Cooling ramp performed at 4 hrs post induction, where T_t was between 22°C and 37°C. **c.** Number of intracellular puncta formed in each cell containing [WT]-40-sfGFP during a cooling ramp from 60°C ➔10°C (green) and imaged isothermally at 22°C. Isothermal analysis performed at 4 hrs post induction, the first timepoint where intracellular puncta were observed. Cooling ramp performed at 4 hrs post induction, but the transition observed was >37°C indicating the possibility of memory.

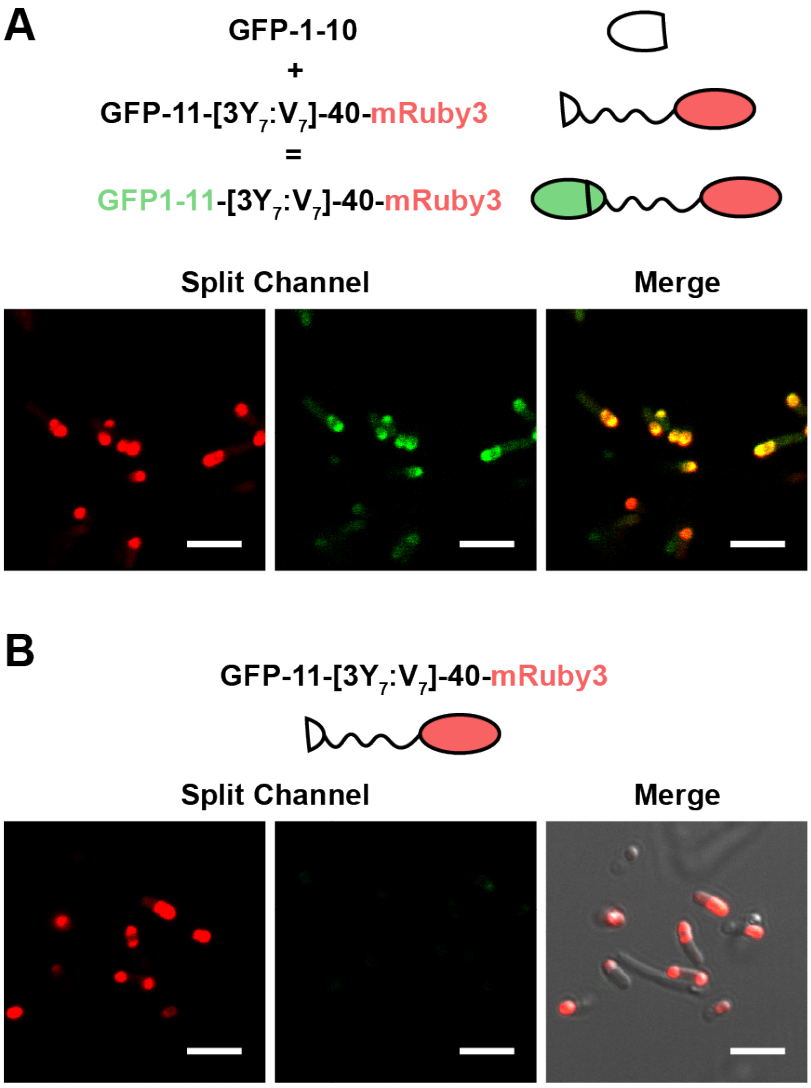

Supplementary Fig. 18. Confocal Microscope Images of Split GFP Recruitment into Intracellular Droplets Related to Fig. 5. a. GFP-11-[3Y_7:V_7]-40-mRuby3 co-expressed in the presence of GFP-1-10 creates fluorescently active GFP only in the interior of the droplet. **b.** In the absence of GFP-1-10 induction, there is little green fluorescent inside the intracellular droplets. Data taken at 22°C. Scale bar = 5 µm.

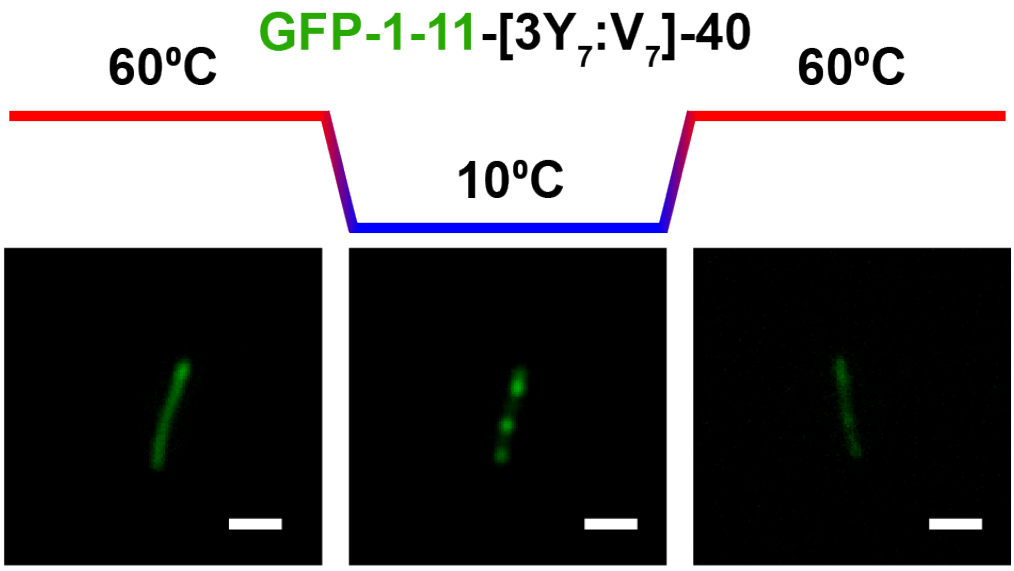

Supplementary Fig. 19. A-IDPs can Modulate the Solubility of an Endogenously Bound Molecule Related to Fig. 6. Upon recruitment of sfGFP into the dense phase, the solubility of the entire complex can be modulated with temperature. Data was collected for 36 hrs post-IPTG induction and 12 hrs post-arabinose induction. Scale bar = 5 μm.

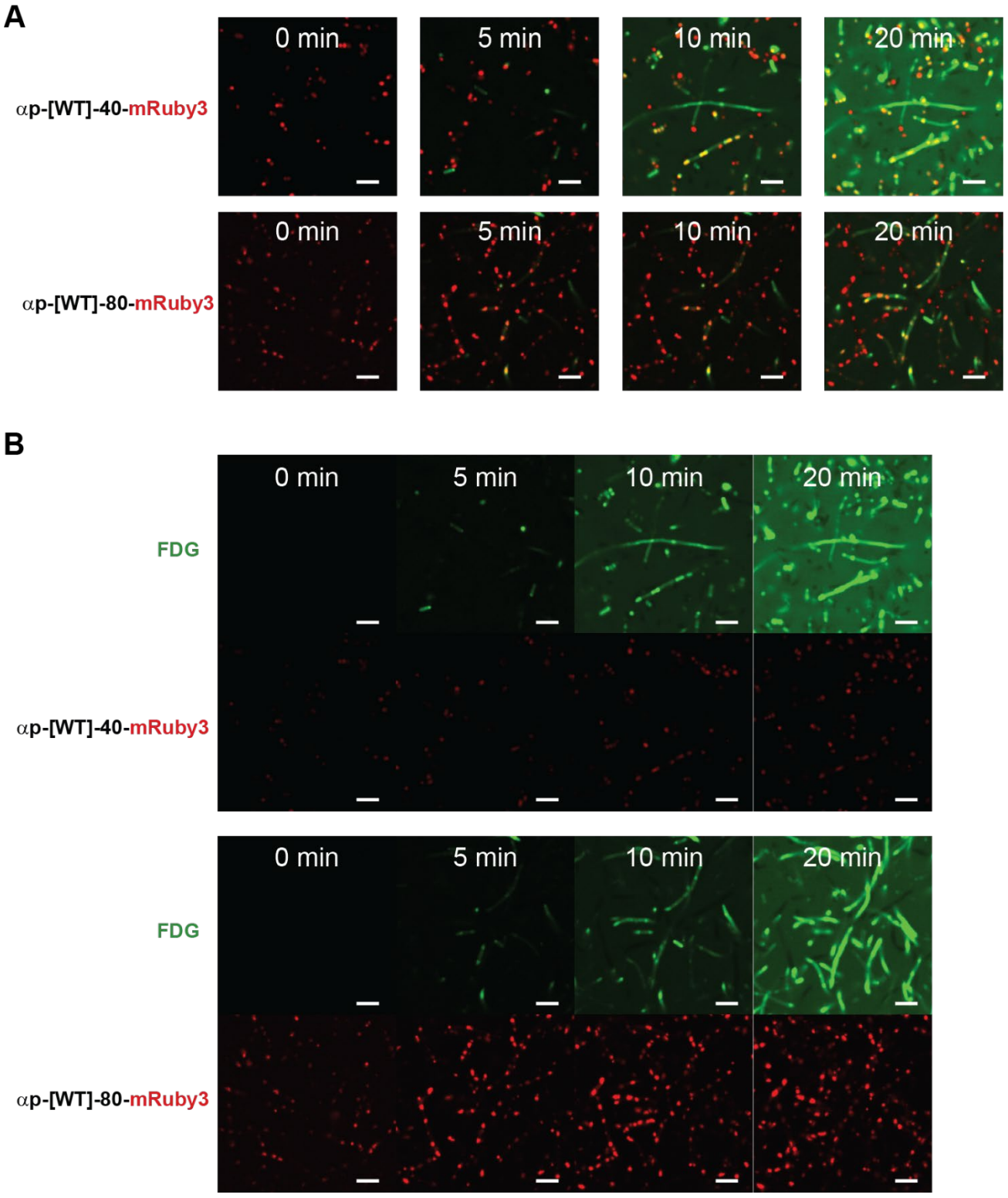

Supplementary Fig. 20. Color Balanced Confocal Microscopy Images of αp-[WT]-40-mRuby3 and αp-[WT]-80-mRuby3 Related to Fig. 7. All scale bars are 5 μm. **a.** Color re-balanced images from Fig. 7a for improved visualization of the intracellular droplets formed by αp-A-IDP-mRuby3 fusions. **b.** Split channel images of αp-[WT]-40-mRuby3 and αp-[WT]-80-mRuby3.

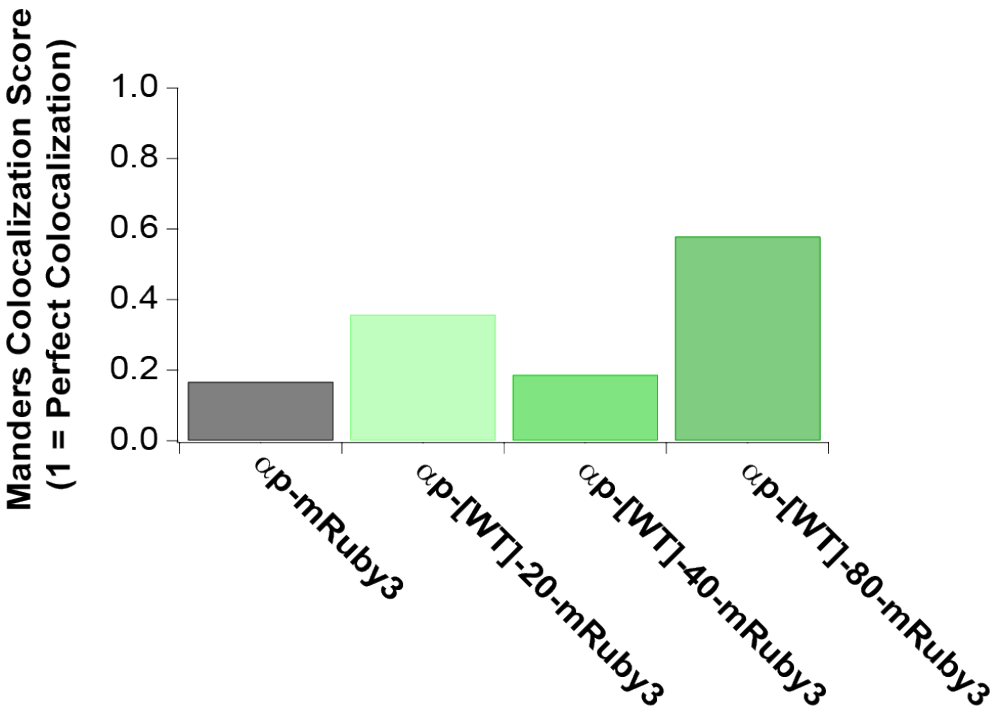

Supplementary Fig. 21. Mander's Colocalization Score Between Converted FDG and Fluorescent Reporter Related to Fig. 7. Data analyzed 30 min after FDG addition. Background threshold was set automatically.

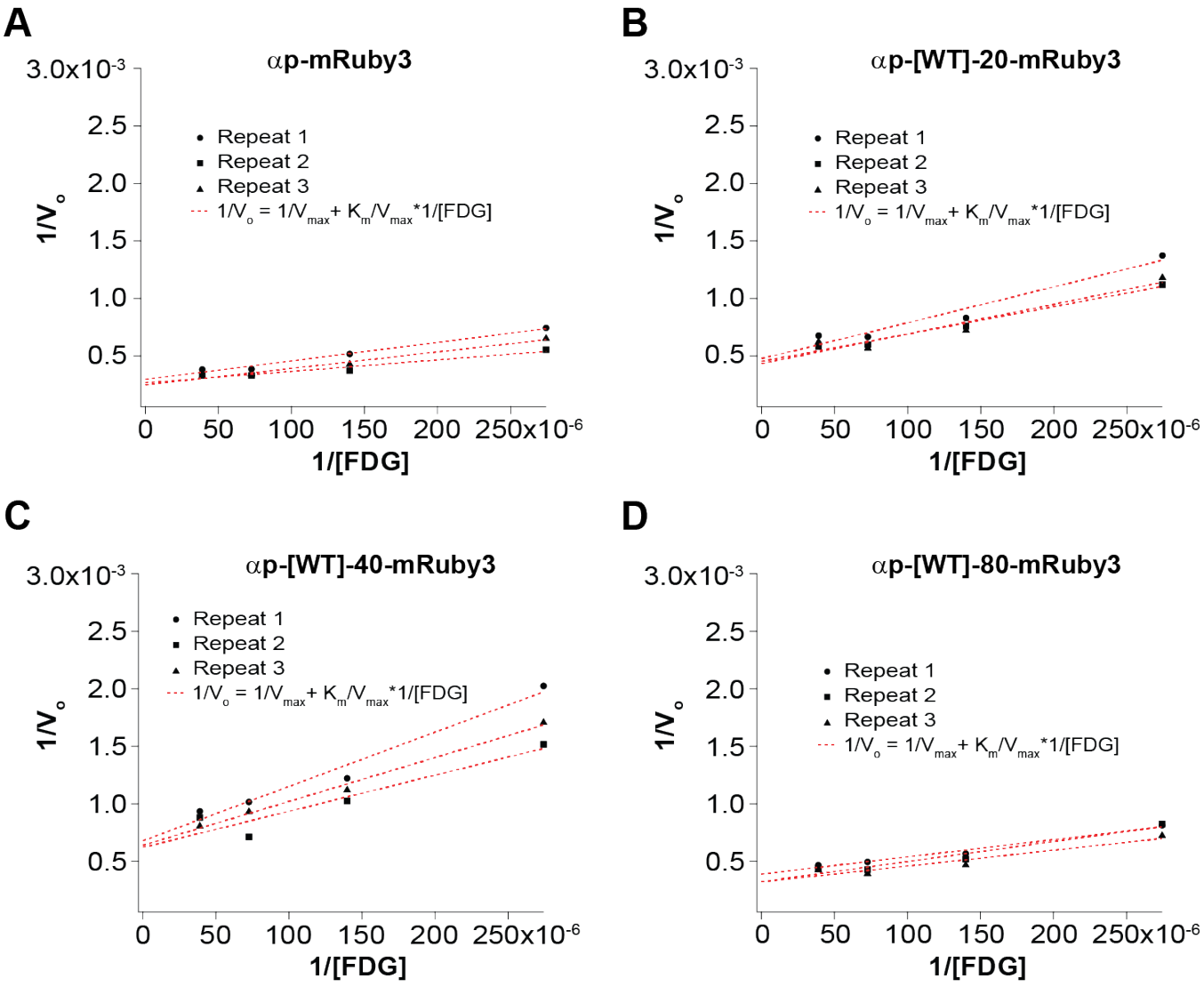

Supplementary Fig. 22. Lineweaver-Burk Plots for Determining K_m and V_{max} Related to Fig. 7. Lineweaver-Burk plots created with variable starting concentrations of FDG for **a.** αp-mRuby3, **b.** αp-[WT]-20-mRuby3, **c.** αp-[WT]-40-mRuby3 and **d.** αp-[WT]-80-mRuby3. Slopes (V_o) were determined from fluorescent generation over the course of 20 minutes. Intercepts and slope were used in the calculation of K_m and V_{max}.

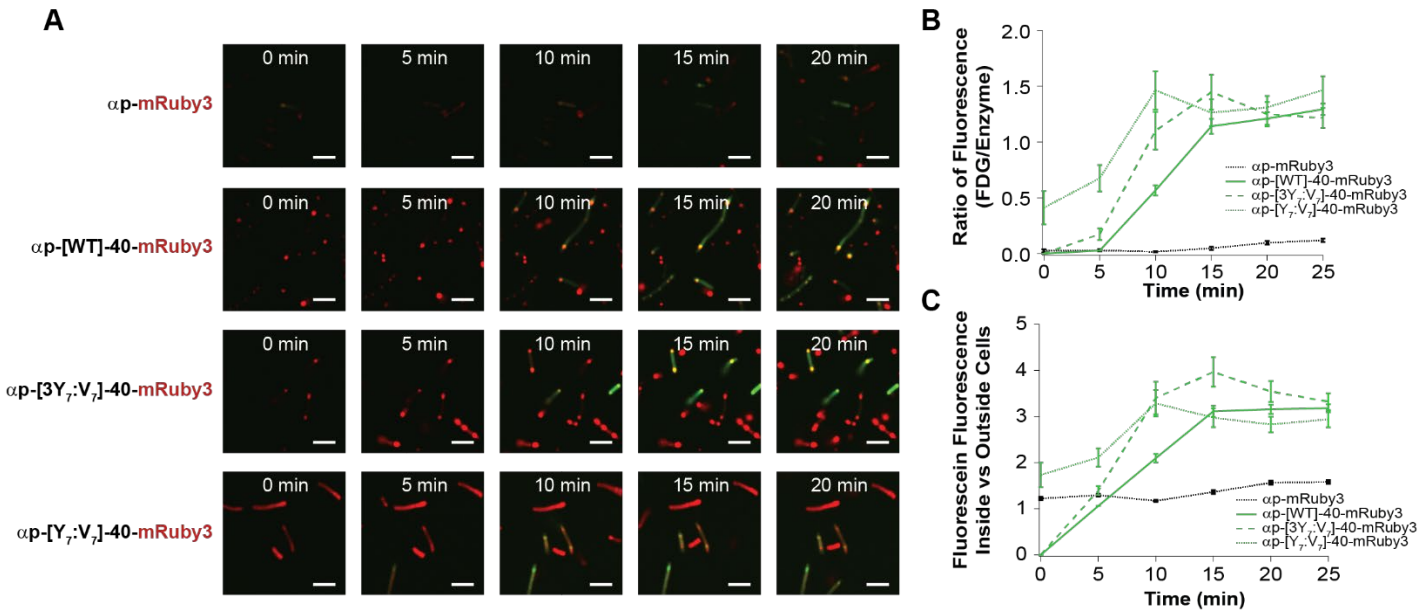

Supplementary Fig. 23. Enzymatic Droplets Formed with Variable Ratio of Aromatic to Aliphatic Ratio Related to Fig. 7. All scale bars are 5μm. **a.** Confocal microscopy images observing the fluorescent conversion of Fluorescein Di-β-D-Galactopyranoside (FDG) of αp-mRuby3, αp-[WT]-40-mRuby3, αp-[3Y_7:V_7]-40-mRuby3 and αp-[Y_7:V_7]-40-mRuby3. Decreasing the aromatic:aliphatic ratio does not increase FDG conversion over time but does change the dynamics of uptake with lower aromatic:aliphatic ratio polypeptides observing higher uptake at earlier timepoints after FDG addition. **b.** Quantified amount of converted FDG intracellularly, normalized to the amount of mRuby3 fluorescence. There is little difference between A-IDPs with different ratios of aromatic:aliphatic content. Error bars indicate standard error of the mean. **c.** All αp-A-IDP-mRuby3 fusions exhibit a higher ratio of FDG fluorescence inside the cell, indicating a greater persistence of fluorescent FDG inside the intracellular space compared to the αp-mRuby3 control. There is little difference between A-IDPs with different levels of aromatic content. Error bars indicate standard error of the mean. n = 300 individual cells from single experiment.

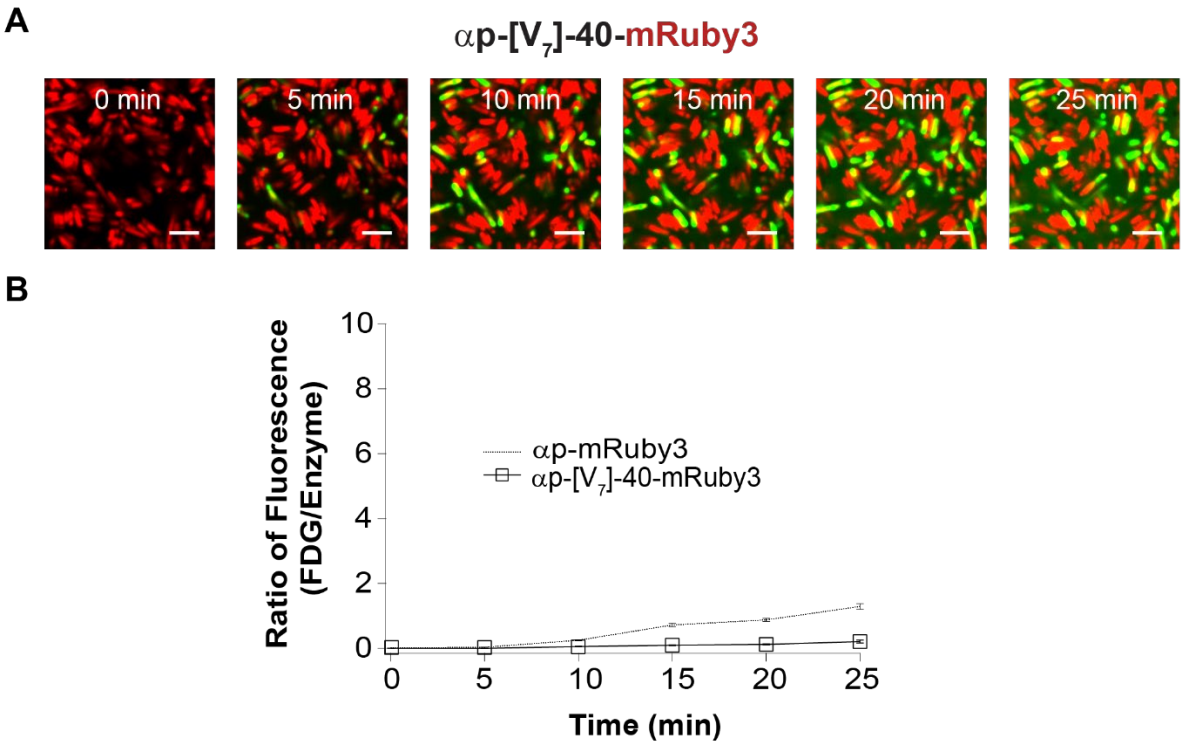

Supplementary Fig. 24. Enzymatic Activity of αp-[V7]-40-mRuby3 Related to Fig. 7. All scale bars are 5 µm. **a.** Confocal microscopy images showing the fluorescent conversion of fluorescein Di-β-D-galactopyranoside (FDG) attached to soluble αp–[V7]-40–mRuby3. **b.** Intracellular concentration of fluorescein produced by catalytic conversion of FDG by αp–[V7]-40–mRuby3, normalized to the mRuby3 fluorescence of each individual cell. The soluble fusion exhibits a lower level of enzymatic activity than all puncta-forming αp-A-IDP fusions. αp-mRuby3 data from Figure 7 redrawn to show scale. Error bars indicate standard error of the mean. n = 300 individual cells from single experiment.

Supplementary Tables:

Supplementary Table 1 – Amino Acid Sequence of A-IDPs with a Single Repeat Motif.

Protein Name	Full Amino Acid Sequence	Amino Acid Number	Molecular Weight (Da)	μM @ 37°C	Image Index
[WT]-20	SKGP-[GRGDSPYS]$_{20}$-GY	166	17004	44.18	1
[WT]-40	SKGP-[GRGDSPYS]$_{40}$-GY	326	33400	0.755	2
[WT]-60	SKGP-[GRGDSPYS]$_{60}$-GY	486	49797	0.044	3
[WT]-80	SKGP-[GRGDSPYS]$_{80}$-GY	646	66193	0.0002	4
[Q$_{5,8}$]-20	SKGP-[GRGDQPYQ]$_{20}$-GY	166	18646	247.9	8
[Q$_{5,8}$]-40	SKGP-[GRGDQPYQ]$_{40}$-GY	326	36685	6.593	9
[Q$_{5,8}$]-60	SKGP-[GRGDQPYQ]$_{60}$-GY	486	54723	1.034	10
[Q$_{5,8}$]-80	SKGP-[GRGDQPYQ]$_{80}$-GY	646	72762	0.241	11
[T$_{5,8}$]-40	SKGP-[GRGDTPYT]$_{40}$-GY	326	34522	0.856	60
[N$_{5,8}$]-20	SKGP-[GRGDNPYN]$_{20}$-GY	166	18085	337.2	12
[N$_{5,8}$]-40	SKGP-[GRGDNPYN]$_{40}$-GY	326	35562	39.18	13
[N$_{5,8}$]-60	SKGP-[GRGDNPYN]$_{60}$-GY	486	53040	4.827	14
[H$_7$]-40	SKGP-[GRGDSPHS]$_{40}$-GY	326	32359	8376.0	61
[H$_7$]-60	SKGP-[GRGDSPHS]$_{60}$-GY	486	48235	286.8	24
[H$_7$]-80	SKGP-[GRGDSPHS]$_{80}$-GY	646	64111	327.0	25
[F$_7$]-40	SKGP-[GRGDSPFS]$_{40}$-GY	326	32760	1.923	62
[Q$_8$]-20	SKGP-[GRGDSPYQ]$_{20}$-GY	166	17825	0.029	38
[Q$_8$]-40	SKGP-[GRGDSPYQ]$_{40}$-GY	326	35042	0.135	39
[Q$_8$]-60	SKGP-[GRGDSPYQ]$_{60}$-GY	486	52260	3.179	40
[Q$_8$]-80	SKGP-[GRGDSPYQ]$_{80}$-GY	646	69478	15.72	41
[Q$_5$]-20	SKGP-[GRGDQPYS]$_{20}$-GY	166	17825	149.0	29
[Q$_5$]-40	SKGP-[GRGDQPYS]$_{40}$-GY	326	35042	7.941	30
[Q$_5$]-60	SKGP-[GRGDQPYS]$_{60}$-GY	486	52260	0.723	31
[Q$_5$]-80	SKGP-[GRGDQPYS]$_{80}$-GY	646	69478	0.086	32
[N$_5$]-40	SKGP-[GRGDNPYS]$_{40}$-GY	326	34481	0.670	21
[N$_5$]-60	SKGP-[GRGDNPYS]$_{60}$-GY	486	51418	0.028	22
[N$_5$]-80	SKGP-[GRGDNPYS]$_{80}$-GY	646	68356	0.004	23
[N$_8$]-20	SKGP-[GRGDSPYN]$_{20}$-GY	166	17544	484.1	18
[N$_8$]-40	SKGP-[GRGDSPYN]$_{40}$-GY	326	34481	16.17	19
[N$_8$]-60	SKGP-[GRGDSPYN]$_{60}$-GY	486	51418	3.748	20
[N$_5$,Q$_8$]-40	SKGP-[GRGDNPYQ]$_{40}$-GY	326	36123	2.449	5
[N$_5$,Q$_8$]-60	SKGP-[GRGDNPYQ]$_{60}$-GY	486	53882	0.176	6

[N_5,Q_8]-80	SKGP-[GRGDNPYQ]$_{80}$-GY	646	71640	0.108	7
[Q_5,N_8]-20	SKGP-[GRGDQPYN]2_0-GY	166	18365	637.5	15
[Q_5,N_8]-40	SKGP-[GRGDQPYN]$_{40}$-GY	326	36123	52.62	16
[Q_5,N_8]-60	SKGP-[GRGDQPYN]$_{60}$-GY	486	53882	13.47	17
[WT]-20-sfGFP	SKGP-[GRGDSPYS]-20-sfGFP	410	44551	216.1	26
[WT]-40-sfGFP	SKGP-[GRGDSPYS]-40-sfGFP	570	60947	3.448	27

Supplementary Table 2 – Amino Acid Sequence of A-IDPs with Multiple Repeat Motifs.

Protein Name	Full Amino Acid Sequence	Amino Acid Number	Molecular Weight (Da)	µM @ 37°C	Image Index
[3$S_{5,8}$:$Q_{5,8}$]-40	SKGP-[GRGDSPYSGRGDSPYSGRGDSPYSGRGDQPYQ]$_{10}$-GY	326	34221	1.600	33
[$S_{5,8}$:$Q_{5,8}$]-40	SKGP-[GRGDSPYSGRGDQPYQ]$_{20}$-GY	326	35042	1.907	34
[$S_{5,8}$:3$Q_{5,8}$]-40	SKGP-[GRGDQPYQGRGDQPYQGRGDQPYQGRGDSPYS]$_{10}$-GY	326	35863	5.062	35
[3Y_7:V_7]-40	SKGP-[GRGDSPYSGRGDSPYSGRGDSPYSGRGDSPVS]$_{10}$-GY	326	32760	24.54	36
[Y_7:V_7]-40	SKGP-[GRGDSPYSGRGDSPVS]$_{20}$-GY	326	32119	815.5	37
[Y_7:3V_7]-40	SKGP-[GRGDSPVSGRGDSPVSGRGDSPVSGRGDSPYS]$_{10}$-GY	326	31479	Unk	N/A
[V_7]-40	SKGP-[GRGDSPVS]$_{40}$-GY	326	30839	Unk	N/A
[3Y_7:A_7]-40	SKGP-[GRGDSPYSGRGDSPYSGRGDSPYSGRGDSPAS]$_{10}$-GY	326	32479	28.46	45
[Y_7:A_7]-40	SKGP-[GRGDSPYSGRGDSPAS]$_{20}$-GY	326	31558	1816	46
[3Y_7:I_7]-40	SKGP-[GRGDSPYSGRGDSPYSGRGDSPYSGRGDSPIS]$_{10}$-GY	326	32900	12.88	47
[Y_7:I_7]-40	SKGP-[GRGDSPYSGRGDSPIS]$_{20}$-GY	326	32400	214.8506	48
[3Y_7:M_7]-40	SKGP-[GRGDSPYSGRGDSPYSGRGDSPYSGRGDSPMS]$_{10}$-GY	326	33080	7.914	49
[Y_7:M_7]-40	SKGP-[GRGDSPYSGRGDSPMS]$_{20}$-GY	326	32761	110.5	50
[3Y_7:H_7]-40	SKGP-[GRGDSPYSGRGDSPYSGRGDSPYSGRGDSPHS]$_{10}$-GY	326	33140	7.125	42
[Y_7:H_7]-40	SKGP-[GRGDSPYSGRGDSPHS]$_{20}$-GY	326	32880	70.86	43

[Y_7:$3H_7$]-40	SKGP-[GRGDSPHSGRGDSPHSGRGDSPHSGRGDSPYS]$_{10}$-GY	326	32619	508.5	44
[$3R_2$:K_2]-40	SKGP-[GRGDSPYSGRGDSPYSGRGDSPYSGKGDSPYS]$_{10}$-GY	326	33120	8.537	51
[R_2:K_2]-40	SKGP-[GRGDSPYSGKGDSPYS]$_{20}$-GY	326	32840	79.88	52
[D_4:E_4]-40	SKGP-[GRGDSPYSGRGESPYS]$_{20}$-GY	326	33681	1.779	53
[$3Y_7$:W_7]-40	SKGP-[GRGDSPYSGRGDSPYSGRGDSPYSGRGDSPWS]$_{20}$-GY	326	33671	0.066	
[Y_7:W_7]-40	SKGP-[GRGDSPYSGRGDSPWS]$_{20}$-GY	326	33901	0.023	
[5G:7P]-40	SKGP[GRPDSPYSGRGDSPYSGRGDSPYSGRGDSPYSPRGDSPYSGRGDSPYSGRGDSPYSGRPDSPYSGRGDSPYSGRGDSPYSGRGDSPYSPRGDSPYSGRGDSPYSGRGDSPYSGRGDSPYSGRPDSPYSGRGDSPYSGRGDSPYSGRGDSPYS]$_2$-GY	326	33801	0.742	54
[G:P]-40	SKGP-[GRPDSPYSGRGDSPYSPRGDSPYSGRGDSPYS]$_{10}$-GY	326	34202	0.728	55
[7G:5P]-40	SKGP-[GRPDSPYSPRGDSPYSGRPDSPYSGRGDSPYSPRGDSPYSGRPDSPYSPRGDSPYSGRGDSPYSGRPDSPYSPRGDSPYSGRGDSPYSPRGDSPYSGRPDSPYSPRGDSPYSGRGDSPYSGRPDSPYSPRGDSPYSGRPDSPYSGRGDSPYS]$_2$-GY	326	34602	0.910	56
[$3Y_7$:V_7]-40-sfGFP	SKGP-[GRGDSPYSGRGDSPYSGRGDSPYSGRGDSPVS]10-sfGFP	570	60307	42.46	28
[$3Y_7$:V_7]-40-UAA	AzF-([GRGDSPYSGRGDSPYSGRGDSPYSGRGDSPVS]-5-AzF)2	323	32660	Unk	N/A

Supplementary Table 3 – Amino Acid Sequence of Fluorescent Protein Reporters

Protein Name	Full Amino Acid Sequence	Amino Acid Number	Molecular Weight (Da)
sfGFP	GKGEELFTGVVPILVELDGDVNGHKFSVRGEGEGDAT NGKLTLKFICTTGKLPVPWPTLVTTLTYGVQCFSRYP DHMKRHDFFKSAMPEGYVQERTISFKDDGNYKTRAE VKFEGDTLVNRIELKGIDFKEDGNILGHKLEYNYNSH NVYITADKQKNGIKANFKIRHNIEDGSVQLADHYQQN TPIGDGPVLLPDNHYLSTQSVLSKDPNEKRDHMVLLE FVTAAGITHGMDELYKELHHHHHHG	246	27785
mRuby3	GVSKGEELIKENMRMKVVMEGSVNGHQFKCTGEGE GRPYEGVQTMRIKVIEGGPLPFAFDILATSFMYGSRTFI KYPADIPDFFKQSFPEGFTWERVTRYEDGGVVTVTQD TSLEDGELVYNVKVRGVNFPSNGPVMQKKTKGWEPN TEMMYPADGGLRGYTDIALKVDGGGHLHCNFVTTYR SKKTVGNIKMPGVHAVDHRLERIEESDNETYVVQREV AVAKYSNLGGGMDELYK	237	26486

Supplementary Table 4 – Number of Phase Separated Domains per *E. coli* as a Function of Induction time (n = 3 images)

Time Post-Induction (hr)	[WT]-20-sfGFP	[WT]-40-sfGFP
2	N/A	1.01 ± 0.02
6	1.03 ± 0.01	1.03 ± 0.03
10	1.13 ± 0.01	1.10 ± 0.09

Supplementary Table 5 – Michaelis-Menten Enzyme Kinetics Parameters (error is standard error of the mean, n = 3).

Protein	V_{max} (FI_{FDG}*min^{-1})	K_m (FI_{FDG})	k_{cat} (min^{-1})	k_{cat}/K_m (FI_{FDG}^{-1}*min^{-1})
αp-mRuby3	3708 ± 183.2	4972 ± 636.3	3.56 ± 0.10	7.43E-04 ± 1.02 E-04
αp-[WT]-20-mRuby3	2165 ± 35.02	5896 ± 380.5	5.10 ± 0.43	8.79E-04 ± 1.16 E-04
αp-[WT]-40-mRuby3	1549 ± 34.75	5988 ± 475.1	5.75 ± 0.13	9.81E-04 ± 9.96 E-05
αp-[WT]-80-mRuby3	2922 ± 174.9	4504 ± 439.7	15.2 ± 0.68	3.45E-03 ± 4.58 E-04

Supplementary Table 6 – Primers Used for pcDNA5 Cloning of [WT]-20-sfGFP.

pcDNA5-Fwd-[WT]-20-sfGFP	CTCACTATAGGGAGACCCAAGCTGGCTAGCATGAGCAAAGGGCCGGGACGC GGCGATAGT
pcDNA5-Rev-[WT]-20-sfGFP	TTAGCCGTGATGGTGATGGTGATGGAGCTCGTTGATTGTCGAGGGCCCTCTA GACTCGAG